

Article

Energy Flexibility Comparison of Different Control Strategies for Zones with Radiant Floor Systems

Ali Saberi-Derakhtenjani ^{1,*}, **Andreas K. Athienitis** ², **Ursula Eicker** ² and **Edwin Rodriguez-Ubinas** ¹¹ Dubai Electricity and Water Authority (DEWA), R&D Centre, Dubai 564, United Arab Emirates; edwin.ubinas@dewa.gov.ae² BCEE Department, Concordia University, Montreal, QC H3G 1M8, Canada; andreask.athienitis@concordia.ca (A.K.A.); ursula.eicker@concordia.ca (U.E.)

* Correspondence: ali.saberi@dewa.gov.ae

Abstract: Radiant floor systems offer significant potential for studying and developing energy flexibility strategies for buildings and their interaction with smart grids. Efficient design and operation of such systems require several critical decisions on design and control variables to maintain comfortable thermal conditions in the space and floor surface temperatures within the recommended range. This study presents a comparison of different control strategies to activate energy flexibility for zones with radiant floor heating systems. The focus of this study is on the zones with radiant floor systems for which the hydronic pipes are located deep in the concrete and therefore, there is a significant thermal lag. A perimeter zone test room equipped with a hydronic radiant floor system in an environmental chamber is used as to validate the modelling methodology. Considering a typical cloudy and cold winter day, three different control strategies for radiant heating were studied based on controlling the zone air temperature, floor surface temperature, and the operative temperature. Then considering morning and evening peak demand periods, the downward and upward energy flexibility are quantified and compared with each other for the different control strategies. It is observed that for the same 2 °C increase or decrease in the setpoint, the control strategy based on the zone air temperature results in the higher flexibility for both downward and upward scenarios compared with the floor surface and operative temperature controls. The effect of increasing window to wall ratio (WWR) is also investigated. Then, also the effect of solar gains on a sunny day on energy flexibility is studied. No significant difference in the upward and downward flexibility is observed. However, the hours of zero heating load are significantly increased due to the contribution from the solar gains.

Keywords: radiant floor heating; energy flexibility; demand response; low-order model

Citation: Saberi-Derakhtenjani, A.; Athienitis, A.K.; Eicker, U.; Rodriguez-Ubinas, E. Energy Flexibility Comparison of Different Control Strategies for Zones with Radiant Floor Systems. *Buildings* **2022**, *12*, 837. <https://doi.org/10.3390/buildings12060837>

Academic Editors: Kheira Anissa Tabet Aoul, Masa Noguchi, Muhammad Tariq Shafiq and Daniel Efurosisibina Attoye

Received: 23 May 2022

Accepted: 10 June 2022

Published: 15 June 2022

Publisher's Note: MDPI stays neutral with regard to jurisdictional claims in published maps and institutional affiliations.



Copyright: © 2022 by the authors. Licensee MDPI, Basel, Switzerland. This article is an open access article distributed under the terms and conditions of the Creative Commons Attribution (CC BY) license (<https://creativecommons.org/licenses/by/4.0/>).

1. Introduction

The increasing global energy demand, the anticipated reduction in available fossil fuels, and the increasing evidence of global warming during the last decades have generated a high interest in renewable energy sources and integration of renewable energy sources into the power grid is increasing rapidly worldwide. However, renewable energy sources, such as wind and solar power, have an inherent variability that can seriously affect the stability of the energy system if they account for a high percentage of the total generation. The flexibility to manage any mismatch between consumption and generation can come from either the supply side through the use of conventional power plants or storage [1–4] or from the demand side [5–8]. The concept of an energy flexible building (EFB) was initiated and studied by IEA EBC Annex 67 [9]. The current definition of building energy flexibility based on the Annex 67 is “the ability to manage building demand and generation according to local climate conditions, user needs, and energy network requirements” [9]. The flexibility of building energy demand profiles is commonly suggested as part of the

solution to alleviate some of the upcoming challenges in the future demand response energy systems [9]. Knowledge of energy flexibility that buildings can provide is important for the design of future smart energy systems, smart grids, and buildings. The knowledge is, however, not only important for utilities but also for companies when developing business cases for products and services supporting the roll out of smart energy networks. Furthermore, it is important for policy makers and government entities involved in the shaping of future energy systems. Radiant floor systems offer significant potential for studying and developing energy flexibility strategies for buildings and their interaction with smart grids. Efficient design and operation of such systems require several critical decisions on design and control variables to maintain comfortable thermal conditions in the space and floor surface temperatures within the recommended range. There have been recent studies on activating and utilizing the energy flexibility of zones with radiant heating systems by means of predictive control strategies [10–12] and through different approaches including frequency domain techniques [13]. However, there have not been any studies on comparing energy flexibility of zones with radiant systems when different types of control strategies and control temperatures are considered. This article investigates this comparison on energy flexibility when different control temperatures are used in a zone with radiant floor heating system with significant thermal mass.

2. Building Energy Flexibility Index

Due to the strong dependence on the boundary conditions and uncertainty in evaluation, energy flexibility quantification in buildings is one of the topics of major interest in current scientific research [14–18].

Buildings can provide different flexibility services to reduce peak loads and shift demand in accordance with local RES production, e.g., utilization of thermal mass [19–22], storage in batteries [23], charging of electric vehicles [24], and adjustability of the HVAC system use [25]. A building energy flexibility index helps to define the amount of energy/power variation over a fixed duration that is available from a building. A well-designed index helps to quantify the flexibility from a building, to improve building design to increase the potential flexibility, to control the building in order to obtain maximum available flexibility when needed, and to compare different systems, designs and operational strategies [26]. The prediction accuracy for the flexibility index within $\pm 10\%$ error is considered optimal for smart grid applications [27].

The use of structural thermal storage (STES) is often suggested as a low-cost key technology to mitigate potential production and distribution capacity issues and to improve the penetration of renewable energy sources. Therefore, a quantitative assessment of the energy flexibility provided by structural thermal energy storage is essential to large scale deployment of thermal mass as in an active demand response (ADR) context. The available storage capacity expresses the amount of energy that can be added to the structure's thermal energy storage (STES) during a specific ADR event. Thus, the heat that can be stored within a dwelling not only depends upon the thermal properties of the building fabric, but also on the properties and actual use of the heating and ventilation systems [14]. Four performance indicators or characteristics for ADR are defined, and quantification methods for the ADR potential of structural thermal storage were presented by Reynders et al. [1]; they are mainly focused on the energy that is reduced/increased over a certain period. Two of these indicators are used in this article, and are briefly described here:

1. Available structural energy storage capacity (C_{ADR}) is defined as the amount of heat that can be added to the structural mass of a building for an active demand response (ADR) event without jeopardizing indoor thermal comfort in a specific timeframe (that is heating above the upper threshold comfort temperature) which can be quantified as [14]:

$$C_{ADR} = \int_0^{t_{ADR}} (Q_{ADR} - Q_{Ref}) dt \quad (1)$$

C_{ADR} is quantified by the integral of the difference between the heating power during this ADR event (Q_{ADR}) and the heating power in normal reference operation (Q_{Ref}), represented by the gray area in Figure 1.

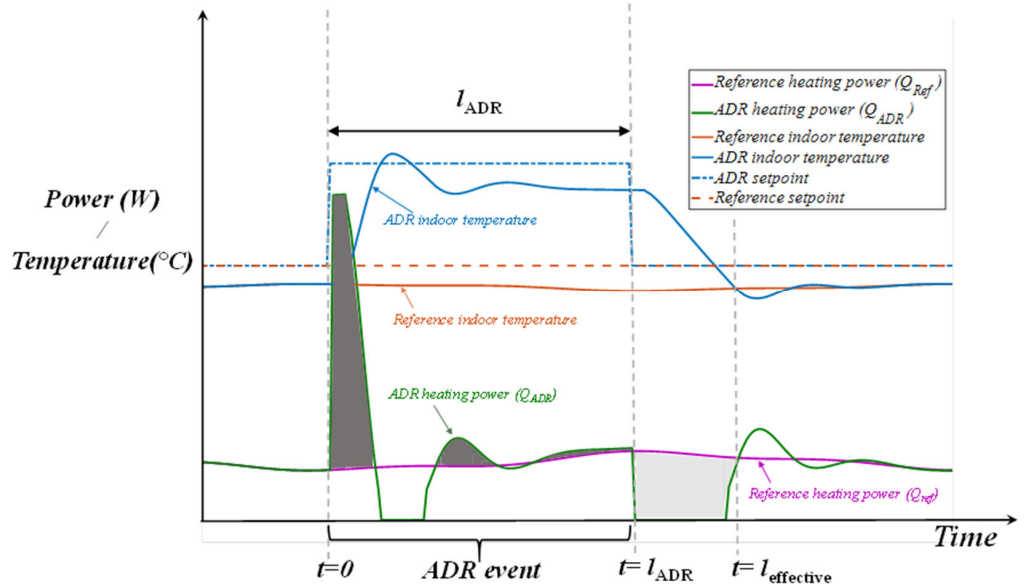


Figure 1. Conceptual representation of the measures used to quantify the available storage capacity and the storage efficiency [13].

The parameter C_{ADR} that is used in this article calculates the building energy flexibility during a desired period which is the active demand response (ADR) event.

2. The storage efficiency (η_{ADR}) represents the fraction of the heat that is stored during the ADR event that can be used subsequently to reduce the heating power needed to maintain thermal comfort [14].

$$\eta_{ADR} = 1 - \frac{\int_0^{l_{effective}} (Q_{ADR} - Q_{Ref}) dt}{\int_0^{l_{ADR}} (Q_{ADR} - Q_{Ref}) dt} \quad (2)$$

Another useful index that quantifies the average power increase/reduction during a specific period of time is the dynamic building energy flexibility index (\overline{BEFI}) developed by Athienitis et al. [26] which is defined as:

$$\overline{BEFI} = \frac{\int_t^{t+l_{ADR}} Q_{Ref} dt - \int_t^{t+l_{ADR}} Q_{ADR} dt}{l_{ADR}} \quad (3)$$

$BEFI$ defines the amount of power variation over a fixed duration that is available from a building. This index is calculated in this article as well.

3. Methodology

The modeling approach used for this study is based on the low-order lumped-parameter thermal network models which are practical for control studies and especially model predictive control [28,29]. In this approach the thermal mass under consideration (radiant floor concrete slab) is discretized into a number of control volumes. Each of the discretized control volumes is represented by a node and considered to be isothermal. Each of the nodes has a lumped thermal capacitance connected to it and thermal conductances connecting it to adjacent nodes. Considering the time interval p and time step Δt , the

general form of the explicit finite-difference model for the nodes with a lumped thermal capacitance can be stated as:

$$T_{i,p+1} = T_{i,p} + \frac{\Delta t}{C_i} \left(Q_i + \sum_j \frac{T_{j,p} - T_{i,p}}{R_{i,j}} \right) \quad (4)$$

where $T_{i,p}$ represents the temperature of node “ i ” at time step “ p ”, $T_{j,p}$ represents temperature of node “ j ” at time step “ p ”, C_i is the thermal capacitance of node “ i ”, $R_{i,j}$ is the thermal resistance between nodes i and j , and Q_i is the heat source at node i . The time step Δt is selected according to this stability criteria:

$$\Delta t \leq \min \left(\frac{C_i}{\sum_j 1/R_{i,j}} \right) \quad (5)$$

where for all the nodes i , the summation is performed for all nodes j connected to the node i .

A model with fewer parameters facilitates setting up the initial conditions which is a key parameter for control studies [28]. When the details of the construction are not known, a low-order grey-box modelling approach is practical and can be developed and calibrated by means of real time data from the building [30]. The models must be accurate enough to provide reliable information but also flexible enough for quick and computationally efficient decision making [31,32] especially in reaction to electric grid’s short notices on the change in price signals.

An important part of a model for zones with radiant floor heating system is the radiative and convective heat transfers, which are inherently nonlinear processes. However, the respective heat transfer coefficients are usually linearized so that the system energy balance equations can be solved with linear algebra techniques and represented with a linear thermal network. In the case of radiant floor heating, this linearization generally introduces less error for the long-wave radiation heat transfer (h_r) than the convection heat exchange between the radiant floor surface and room air (h_{cf}) [33]. For example, in the case of radiant floor heating where usually the floor is hotter than the air and the heat flow is upward h_{cf} is in the order of 3 W/(m²K) while for a cold floor and warmer air it is in the order of 1 W/(m²K) [33]. Therefore, usually a certain amount of calibration for the convection heat exchange between the radiant floor and room air is required for a model especially when considering the low-order models. Heat flow upwards h_{cf} can be calculated as [34]:

$$h_{cf}(t) = 1.52(T_{\text{floor}}(t) - T_{\text{air}}(t))^{1/3} \quad (6)$$

where T_{floor} is the floor surface temperature and T_{air} is the zone air temperature.

A well-calibrated low-order model can accurately capture the most important thermal dynamics of a zone with a radiant floor heating system. This modeling technique was validated through experiments in a Solar Simulator/Environmental Chamber and PZTC test facility. The Solar Simulator/Environmental Chamber (SSEC) laboratory is an experimental facility located at Concordia University in downtown Montreal, Canada. This facility allows accurate and repeatable testing of solar systems and advanced building envelopes under standard test conditions with simulated solar radiation and indoor plus outdoor conditions. The temperature test range of the environmental chamber is -40°C to $+50^{\circ}\text{C}$. Two solar simulators (large-scale and mobile) are designed to emulate solar radiation to test solar systems such as PV and PV/T modules, solar air collectors, solar water collectors, and building-integrated solar systems. The perimeter zone test cell (PZTC) is a 3 m × 3 m × 3 m office placed inside the Solar Simulator/Environmental Chamber laboratory, and it has a radiant floor heating/cooling system. The side and back walls and ceiling consists of 10 cm of insulation with thermal resistance of 5.64 m²K/W. The front wall is designed to be modifiable to test different facades and glazing systems and currently has a thin cover with 0.88 m²K/W thermal resistance. The floor is fabricated of

an approximately 8 cm thick concrete slab, with the piping at the bottom of the concrete and insulation of $7.4 \text{ m}^2\text{K/W}$ under the slab. Thermal properties of the concrete are shown in Table 1.

Table 1. Thermal properties of concrete.

Properties	
Thermal conductivity	$1.7 \text{ W}/(\text{m}\cdot\text{K})$
Specific heat	$800 \text{ J}/(\text{kg}\cdot\text{K})$
Density	$2010 \text{ kg}/\text{m}^3$

The pipes of the radiant floor system are fabricated of conventional cross-linked polyethylene (PEX) and have an external diameter of 1.75 cm. The pipes are installed in a foam matrix of insulating material that also facilitates keeping them in place. The pipes are spaced at 15 cm. Figure 2 shows the piping configuration of the radiant floor before the concrete was poured (left), during pouring of concrete, and the final look of the radiant floor slab (right).



Figure 2. Radiant floor piping before (left), during (middle), and after (right) pouring the concrete.

A mechanical room provides controlled flow rate of the fluid (propylene-glycol and water mixture) for the radiant floor. The schematic of the environmental chamber and PZTC is shown in Figure 3.

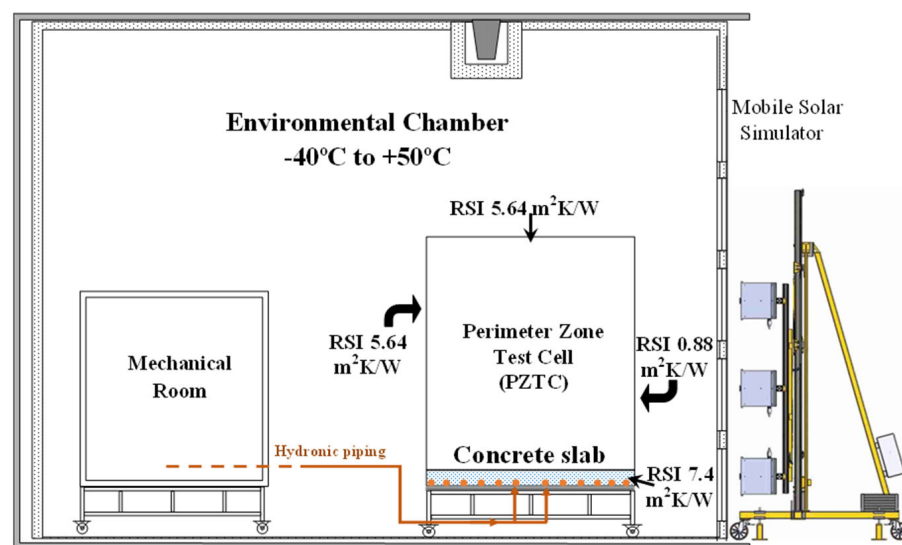


Figure 3. Schematic of SSEC with PZTC and radiant floor.

A low-order (second-order) grey-box model was developed by the authors for the PZTC. Figure 4 shows thermal network model of the PZTC. To study the effect of variable window to wall ratio (WWR) on energy flexibility, initially 50% WWR was considered for the front façade of the PZTC.

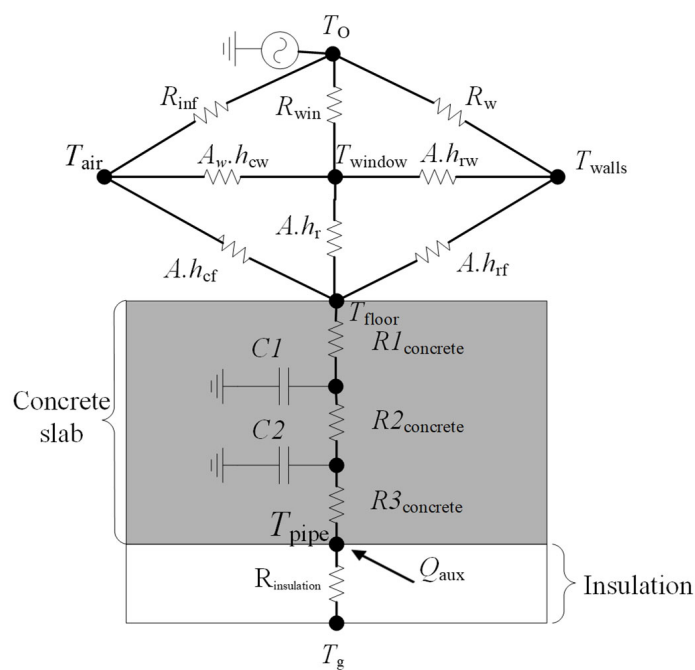


Figure 4. Thermal network model of the zone.

As mentioned before, the floor convective heat transfer can vary significantly depending on the temperature difference between the floor surface temperature and the air in the zone. Therefore, an objective function is defined to find the effective values of h_{cf} so that the floor surface temperature calculated from the simulations ($T_{\text{floor, simulated}}$) matches with experiment ($T_{\text{floor, measured}}$) as accurately as possible. Therefore, the objective function is defined using the Euclidean norm of the difference as:

$$\text{Min} J = \|T_{\text{floor, simulated}} - T_{\text{floor, measured}}\| \quad (7)$$

Optimization was performed in MATLAB using the fmincon function which uses the simplex algorithm. The optimization result is shown in Figure 5.

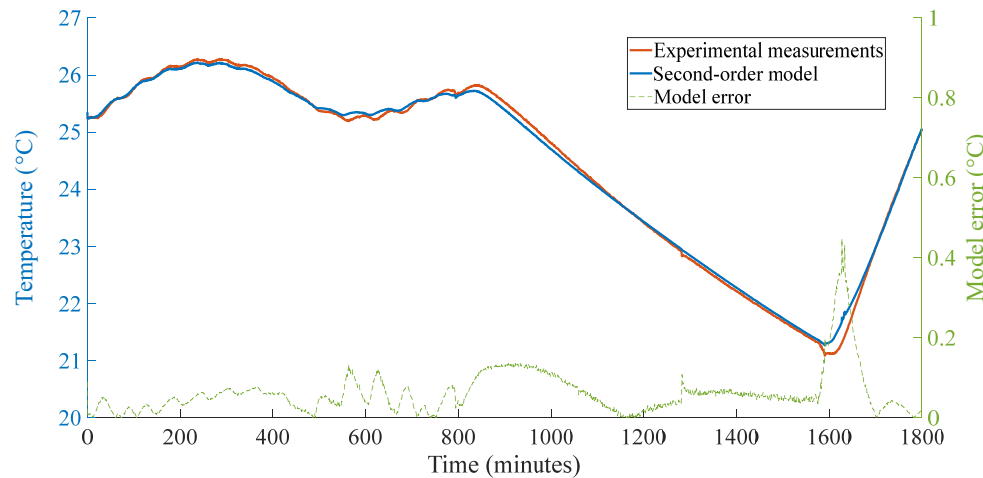


Figure 5. Second-order grey-box model versus experimental measurements and model error.

As observed, a well-calibrated low-order model can capture thermal dynamics of a zone that contains radiant floor heating system with a good accuracy and the maximum error between the model and the measurements is about 0.45°C . However, for the majority of the time the model error is less than 0.1°C . Moreover, another fitness metric is the

coefficient of variance of the root mean square error (CV-RMSE) shown in Equation (8) in which T_i is the measured temperature and \hat{T}_i is the simulation temperature, n shows the total number of observation and \bar{T} is the average of all measurements.

$$CV - RMSE(\%) = 100 \times \frac{\sqrt{\sum_{i=1}^n (T_i - \hat{T}_i)^2 / n}}{\bar{T}} \quad (8)$$

According to ASHRAE Guideline 14 [35], a model should not exceed a CV-RMSE of 30%. The CV-RMSE is calculated here to be 15%.

The validated low-order model is used in the following section to study different control strategies based on the floor surface temperature, zone air temperature, and operative temperature. The quantified energy flexibility for each case is compared with each other. An external façade with 50% WWR double-glazed, low-e windows was considered for the PZTC. The heating is controlled by the proportional control strategy which is defined as:

$$Q_{aux}(t) = K_p(T_{sp}(t) - T_{control}(t)) \quad (9)$$

where K_p is the proportional constant, T_{sp} is the desired setpoint temperature and $T_{control}$ is the controlled temperature which here is the floor surface (T_{floor}), air (T_{air}), and operative (T_{op}) temperatures, respectively.

4. Results

This section presents the simulation results of controlling different temperatures in the thermal zone and their respective energy flexibility by means of the validated second-order model. The outdoor condition is considered as a cloudy cold winter day in Montreal as shown in Figure 6. The goal here is to evaluate and quantify the downward and upward energy flexibility for the evening and morning peak demand periods respectively for a typical cold winter day. Therefore, in order to let the model stabilize from the initial conditions, two identical days (48 h) were considered for simulations first.

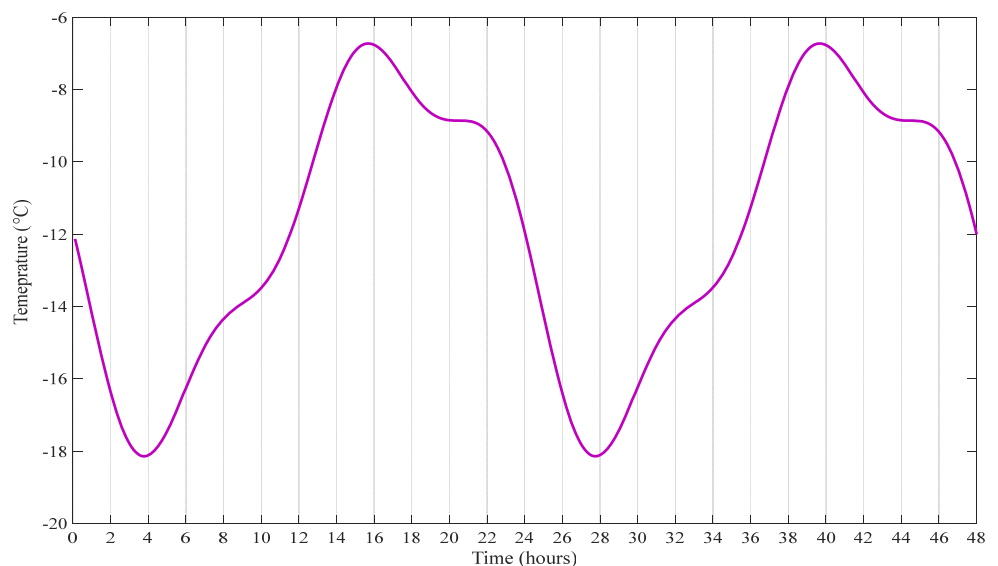


Figure 6. Outdoor temperature profile.

Next section presents results of floor surface temperature control starting from the reference setpoint profile and then showing the results for the downward and upward flexibility strategies.

4.1. Floor Surface Temperature Control

Figure 7 shows the heating load profile for the floor surface temperature control considering the constant, reference setpoint of 26 °C. It can be observed that the heating load changes during this 48-h period and a relatively smooth load profile is seen.

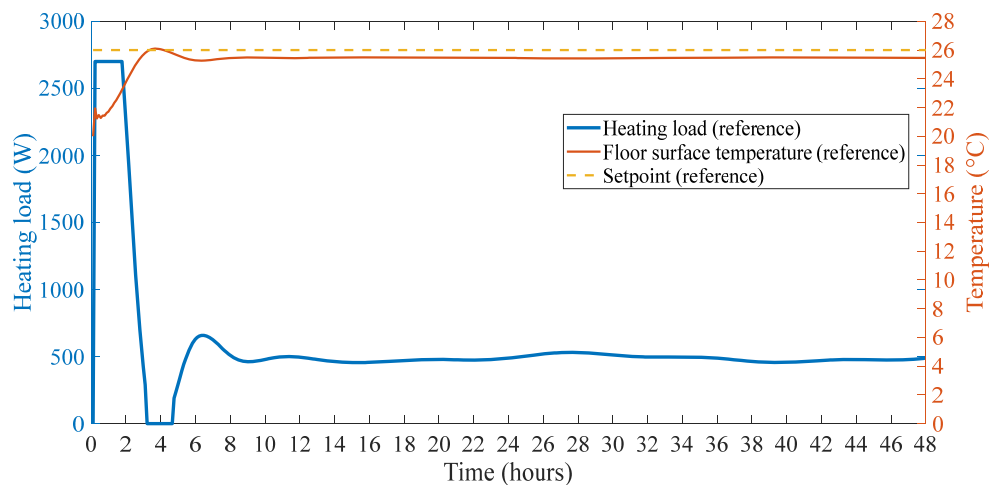


Figure 7. Reference case for floor surface temperature control.

Considering that a higher than usual penalty signal from the grid is observed on the first day during the evening peak demand period, which is around 4 to 8 p.m., if we perform the reactive control and lower the surface temperature setpoint by 2 °C (from 26 °C to 24 °C) during that period, the following change in the heating load is observed and shown in Figure 8:

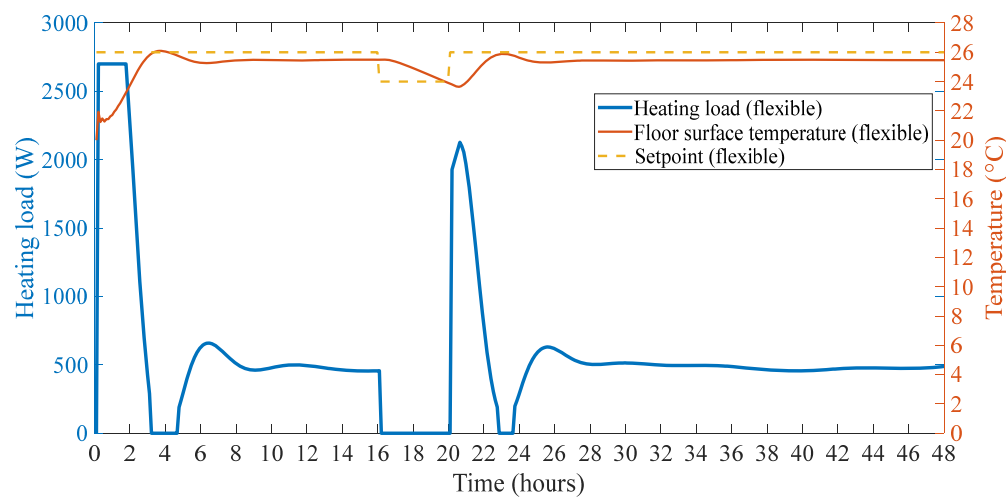


Figure 8. Downward flexible case for floor surface temperature control.

As observed, by lowering the setpoint, the heating load drops to zero due to the thermal mass of the concrete slab. For this 4 h period, the downward flexibility, $C_{ADR,D}$ is calculated from Equation (1) and is equal to 198 Wh/m².

With this control strategy, the zone air and operative temperatures stay within the comfort range as observed in Figure 9.

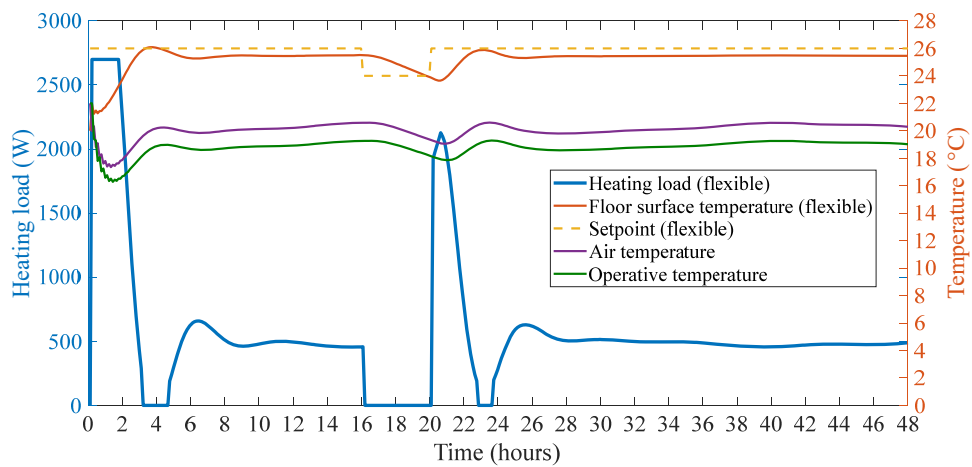


Figure 9. Zone air and operative temperatures profiles with surface temperature control strategy.

The $BEFI_D$ for this downward flexibility event is 457 W or $BEFI_D = 50 \text{ W/m}^2$. For the next day, the morning peak period of 6–9 a.m. (hours 30–33 in the figure), a predictive strategy is considered to preheat the slab by increasing the setpoint to 28 °C at night for 3 h (from 27 to 30) just before the morning peak demand period. As observed in Figure 10, then the heating load and energy consumption is zero during the peak demand period and even one hour after that (4 h in total). The upward flexibility for this 3 h period is calculated as $C_{ADR,U} = 222 \text{ Wh/m}^2$ and the $BEFI_U = 76 \text{ W/m}^2$.

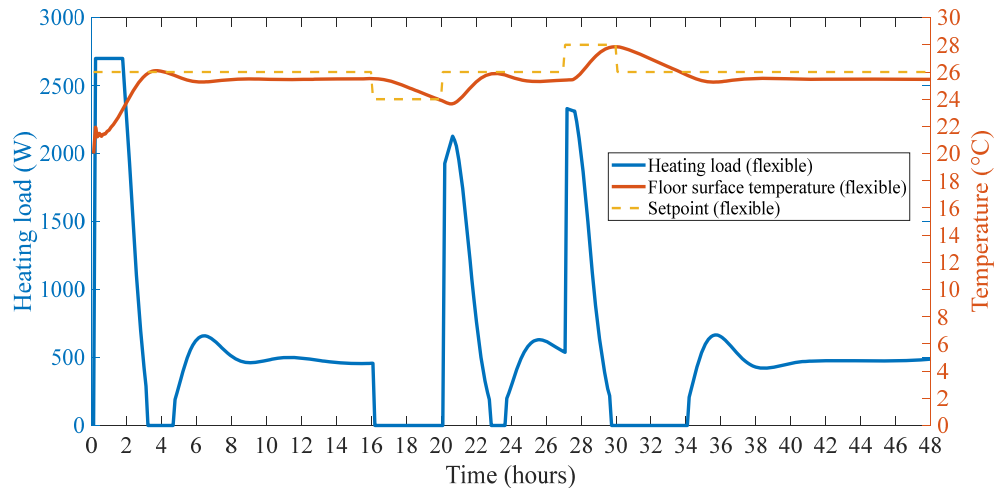


Figure 10. Upward flexible case for floor surface temperature control.

The storage efficiency for the rest of the day is calculated as $\eta_{ADR} = 91\%$. This means that for the rest of the day, 91% of the stored thermal energy during the morning ADR event, equal to 202 Wh/m², is used to further change and decrease the heating load during the rest of the day compared with the reference case.

4.2. Air Temperature Control

If we consider the zone air temperature control instead of the floor surface, the heating load profile for the reference setpoint of 22 °C is shown in Figure 11.

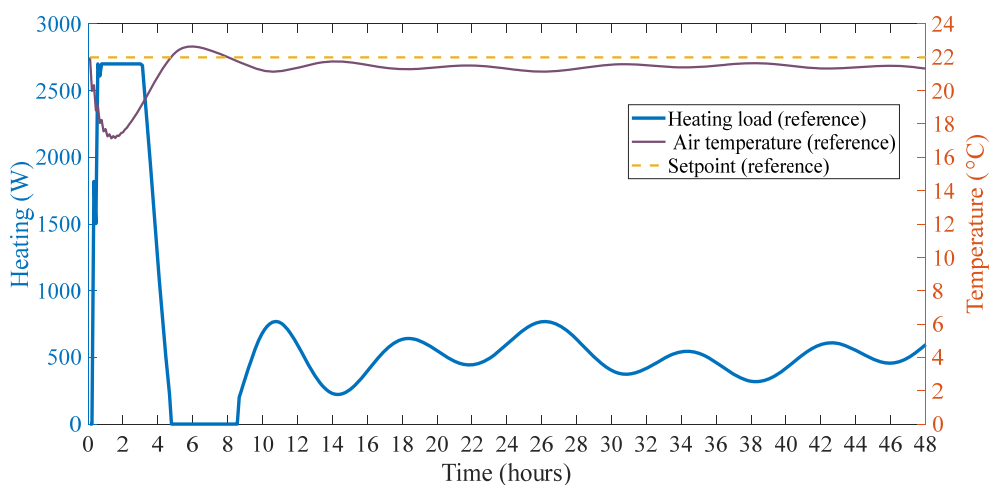


Figure 11. Reference case for air temperature control.

Comparing Figures 10 and 11, we can see more fluctuations in the heating load profile for the air temperature control compared with the floor surface which is due to the much lower thermal mass of zone air compared with the concrete slab. Now, applying the same strategy, If the air temperature setpoint is decreased by 2 °C (to 20 °C) during the first day evening peak demand period (hours 16–20), Figure 12 shows the heating load profile.

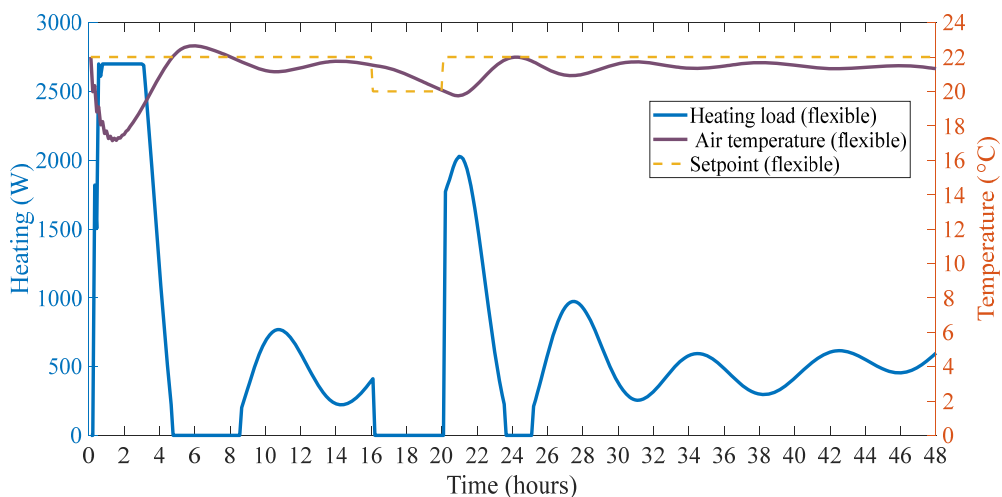


Figure 12. Downward flexible case for air temperature control.

For this case, $C_{ADR,D}$ for the 4 h period is equal to 247 Wh/m^2 which considering the same 2 °C drop in the setpoint, shows about a 25% increase compared with the previous case of floor surface temperature control (194 Wh/m^2). Furthermore, the average reduction in heating power is equal to: $BEFI_D = 63 \text{ W/m}^2$.

Considering the preheating before the next day's morning peak period (hours 30–33), the heating profile is shown in Figure 13. The upward flexibility for this case is calculated as $C_{ADR,U} = 313 \text{ Wh/m}^2$ which is 40% higher compared with the case of floor surface temperature control (222 Wh/m^2).

It is observed that this control strategy based on zone air temperature also results in 5.5 h of zero heating load after the upward flexibility event compared with the 4 h with floor surface temperature control. The storage efficiency for the rest of the day is calculated as $\eta_{ADR} = 78\%$, meaning that after the morning ADR event, $313 \times 0.78 = 244 \text{ Wh/m}^2$ is used to further reduce the heating load for the rest of the day. The average increase in

heating power during this ADR event is equal to $BEFI_U = 104 \text{ W/m}^2$ which shows about a 37% increase compared with the previous case with floor surface temperature control.

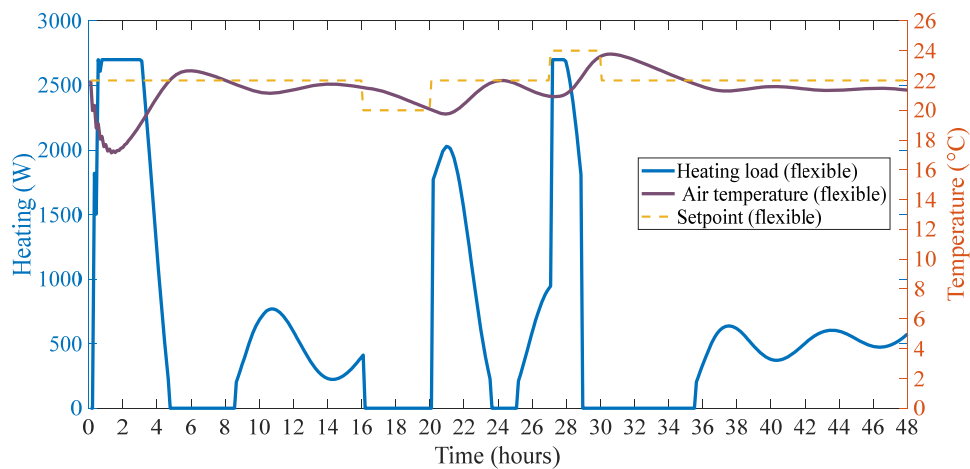


Figure 13. Upward flexible case for air temperature control.

Another important observation in Figure 13 is that during the upward ADR event, the heating load is stopped around hour 29 while the air temperature did not reach the threshold of 22 °C. The reason for this is that in the radiant heating system, there is a limitation for the floor surface temperature to not exceed 29 °C based on the ASHRAE standard [35]. Therefore, as seen in Figure 14, when the floor surface reaches 29 °C, the heating is stopped automatically.

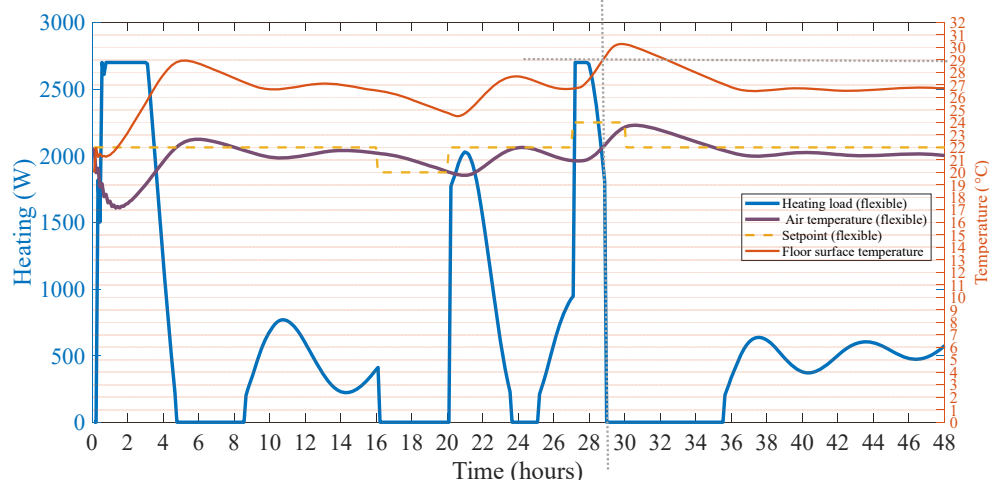


Figure 14. Stoppage of heating when floor surface reaches 29 °C.

4.3. Operative Temperature Control

Based on ASHRAE standard 55, the operative temperature of a zone is defined as [35]:

$$T_{\text{op}} = \frac{T_{\text{air}} + T_{\text{mr}}}{2} \quad (10)$$

where T_{mr} is the mean radiant temperature and T_{air} is the zone air temperature.

For the operative temperature control, Figure 15 shows the heating load profile for the reference setpoint of 21 °C.

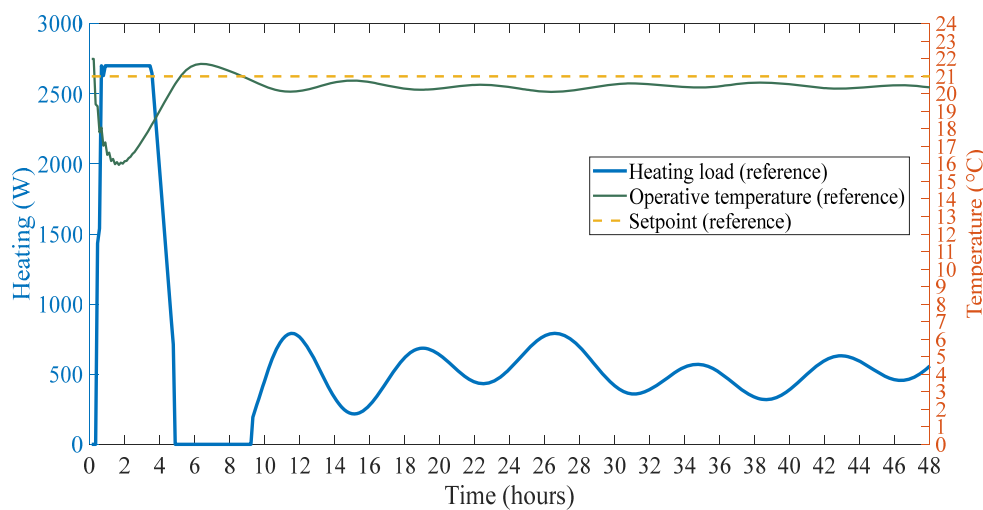


Figure 15. Reference case for the operative temperature control.

Similar to the previous cases, for the downward and upward flexible case, the heating load is shown in Figure 16.

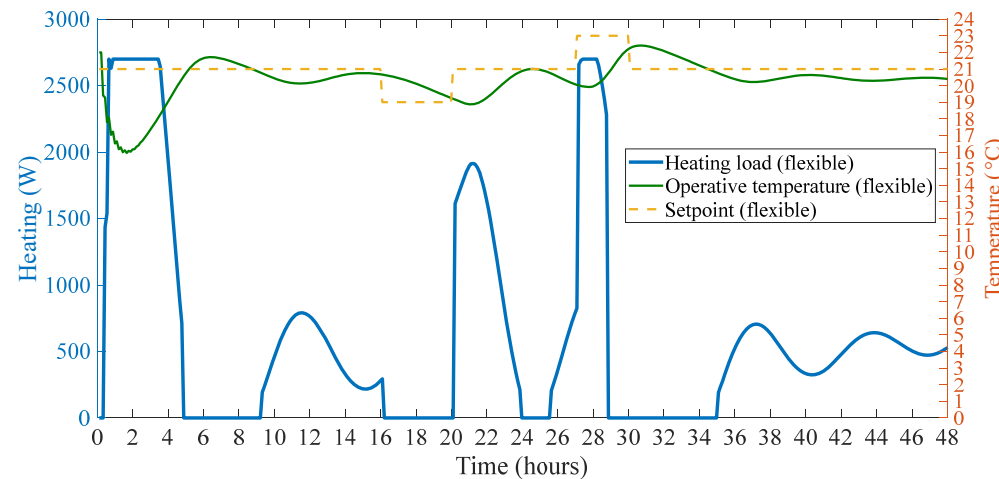


Figure 16. Downward and upward flexible case for the operative temperature control.

For the downward flexible case, $C_{ADR,D} = 240 \text{ Wh/m}^2$ and $BEFI_D = 61 \text{ W/m}^2$; and for the upward flexible case, $C_{ADR,U} = 294 \text{ Wh/m}^2$, and $BEFI_U = 97 \text{ W/m}^2$. The storage efficiency for the rest of the day is calculated as $\eta_{ADR} = 73\%$.

Table 2 sums up the results for different cases and control strategies.

Table 2. Comparison of different control strategies.

	Control Strategies		
	Floor Surface Temp	Air Temp	Operative Temp
Downward Flexibility ($C_{ADR,D}$), Average power reduction ($BEFI_D$)	198 Wh/m ² , 50 W/m ²	247 Wh/m ² , 63 W/m ²	240 Wh/m ² , 61 W/m ²
Upward Flexibility ($C_{ADR,U}$), Average power increase ($BEFI_U$), η_{ADR} , Zero load hours	222 Wh/m ² , 76 W/m ² , 91%, 4 h	313 Wh/m ² , 104 W/m ² , 78%, 5.5 h	294 Wh/m ² , 97 W/m ² , 73%, 4.5 h

Comparing the three cases, it is observed that for the same reduction or increase of 2 °C in the corresponding setpoint, the air temperature control strategy results in higher C_{ADR} and $BEFI$ and therefore higher energy flexibility (both upward and downward) as well as longer hours of zero load compared with floor surface and operative temperature control.

4.4. Effect of Increasing the WWR

The effect of increasing the window area of the exterior façade on the energy flexibility was investigated. The WWR increased from 50% to 75%. Figure 17 shows the comparison of the two variations for the reference case of air temperature control.

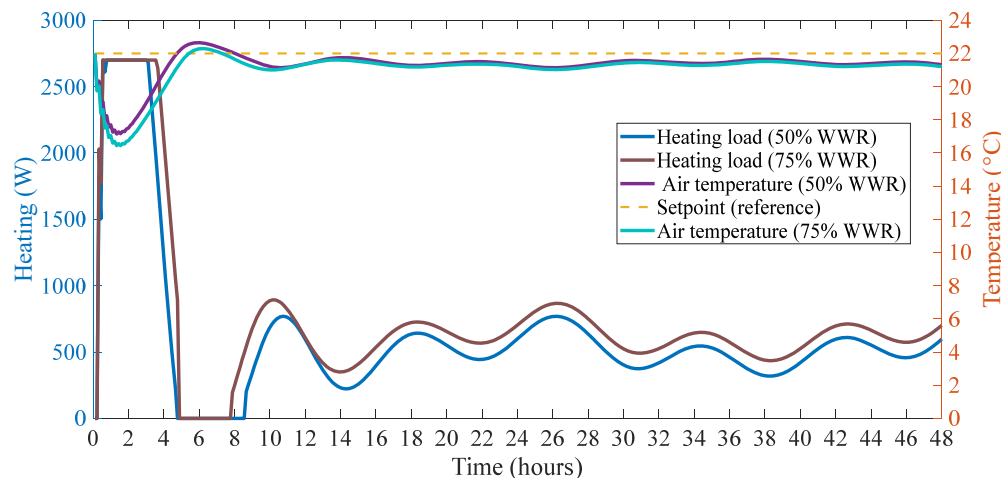


Figure 17. Comparison of air temperature control reference case for two WWRs.

As expected, there is a noticeable increase in the heating load.

Considering the flexible setpoint, the heating load for the 75% WWR is shown in Figure 18.

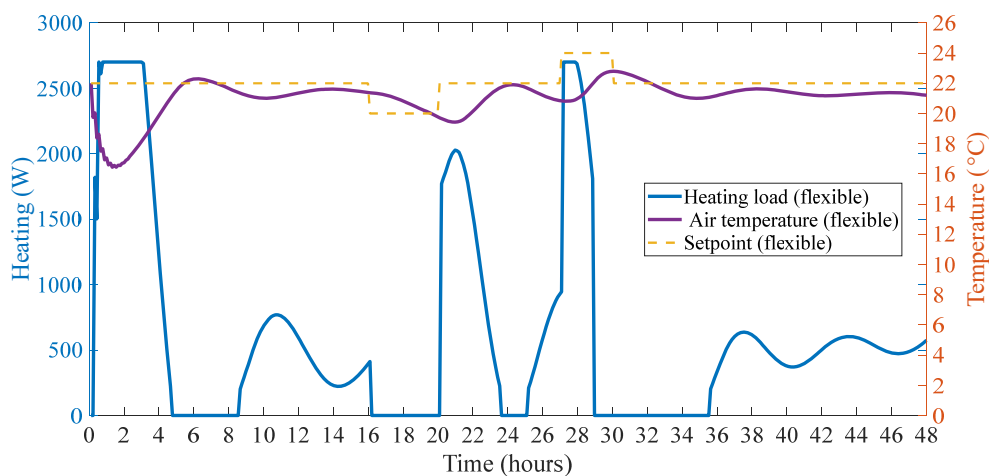


Figure 18. Downward and upward flexibility for the air temperature control and 75% WWR.

The downward and upward energy flexibilities for this case are: $C_{ADR,D} = 289 \text{ Wh/m}^2$ and $C_{ADR,U} = 182 \text{ Wh/m}^2$. Therefore, as the heating load is increased with increasing WWR, the downward flexibility is increased by 17%. However, in the case of upward flexibility, a decrease of 42% (from 313 Wh/m²) was observed.

4.5. Effect of Solar Gains

The previous section simulations were performed considering a cloudy day. Having solar gains through a part of the window on a part of the floor can have a noticeable impact

on the heating load and indoor temperature and cause significant fluctuations. To evaluate this impact, a half sinusoidal solar radiation profile shown in Figure 19 was considered and it is assumed that only a small portion of it passes through part of the window and heats part of the floor.

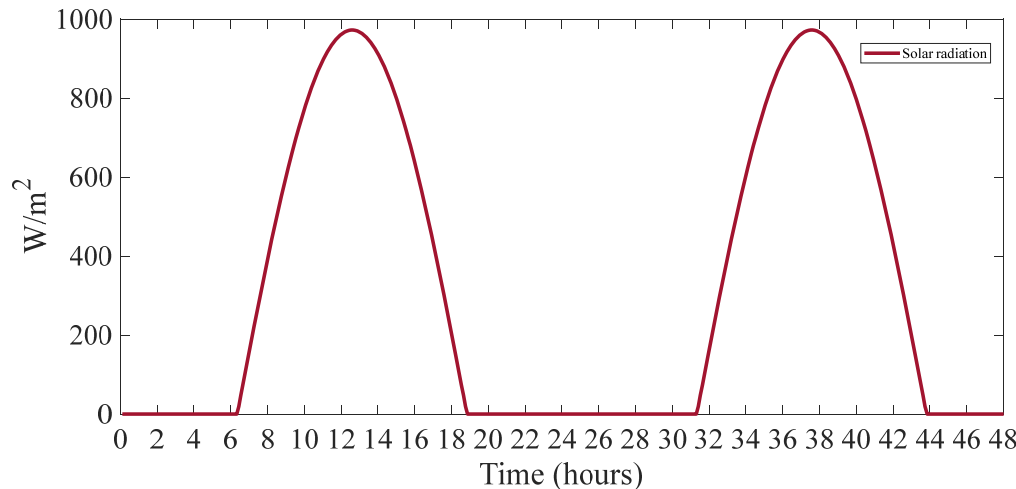


Figure 19. Solar radiation profile for a sunny day.

Figure 20 shows the reference profile for floor surface temperature control for this case.

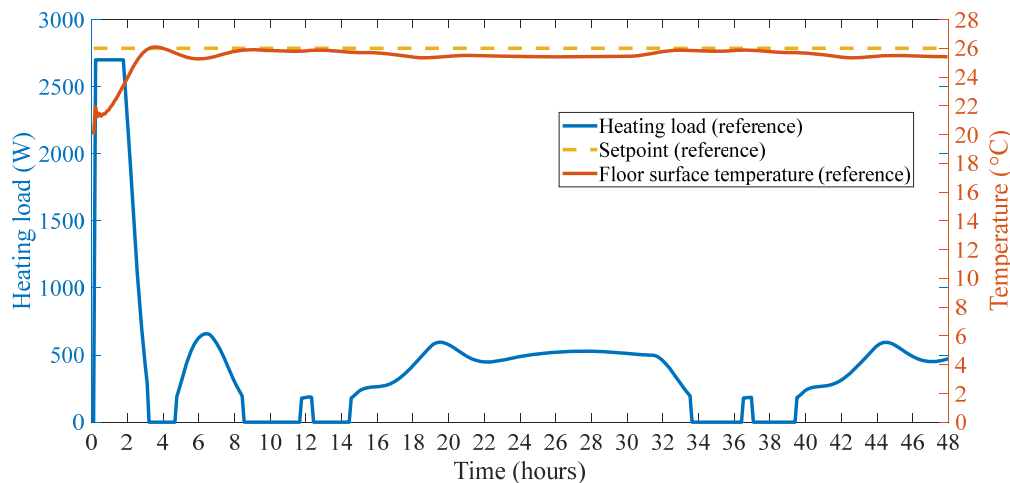


Figure 20. Reference case for floor surface temperature control with solar radiation.

As observed, there are more fluctuations in the floor surface temperature and the heating load profile which shows a significant impact of the solar gain. We can see that for the hours between 9 and 14.5 and for the next day between the hours 33.5 and 39.5, very little heating is required.

For the flexible setpoint case, Figure 21 shows the load profile for the downward and upward flexibility.

For the downward flexibility case, $C_{ADR,D} = 185 \text{ Wh/m}^2$ which is 6.5% less compared with the cloudy day (198 Wh/m^2) since the heating load is also smaller. Moreover $BEFI_D = 47 \text{ W/m}^2$, which is also 6% lower than the one for the cloudy day (50 W/m^2).

For the upward flexibility, $C_{ADR,U} = 231 \text{ Wh/m}^2$ which is slightly higher (4%) than the cloudy day (222 Wh/m^2) and the storage efficiency for the rest of the day is $\eta_{ADR} = 88\%$. Furthermore, the average increase in power $BEFI_D = 76 \text{ W/m}^2$ which is the same as the cloudy day.

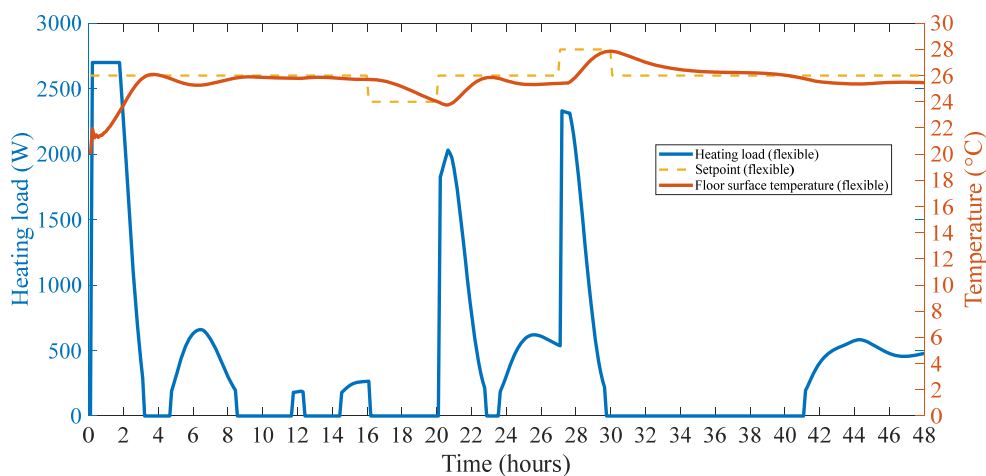


Figure 21. Flexible heating load profile for floor surface temperature control.

As the above analysis showed, there is no major difference between the flexibility indicators and the difference is less than 7% between a cloudy and a sunny day. However, a major difference is observed during the hours of the zero heating load after the upward flexibility event. As shown in Figure 21, about 11 h (30–41) of zero heating load is achieved with the aid of solar gains. The use of solar gains should be considered with careful considerations of shades as it can seriously fluctuate the indoor temperature and consequently the occupant comfort.

5. Discussion and Conclusions

This study presented a comparative analysis of energy flexibility for different control strategies for zones with radiant floor heating systems with significant thermal mass. It was observed that with every control strategy, a noticeable amount of energy flexibility is achieved by decreasing or increasing the control temperature setpoint during or before the high price signal (peak demand) period. For the control strategy based on the floor surface temperature, downward flexibility of $C_{ADR,D} = 198 \text{ Wh/m}^2$ and the average power reduction in $BEFI_D = 50 \text{ W/m}^2$ was achieved during the evening peak demand period. The upward flexibility for this case was $C_{ADR,U} = 222 \text{ Wh/m}^2$ for the 3 h before the morning peak demand period, and the average increase in $BEFI_U = 76 \text{ W/m}^2$ in power was observed. The storage efficiency of $\eta_{ADR} = 91\%$ was obtained for the rest of the day after the upward flexibility event, meaning about 202 Wh/m^2 was used subsequently to reduce the heating load.

For the control strategy based on the air temperature control, the calculated variables were $C_{ADR,D} = 247 \text{ Wh/m}^2$ and $BEFI_D = 63 \text{ W/m}^2$ for the downward case, and $C_{ADR,U} = 313 \text{ Wh/m}^2$ and $BEFI_U = 104 \text{ W/m}^2$ for the upward case. The storage efficiency for this case was $\eta_{ADR} = 78\%$ for the rest of the day after the upward flexibility event, meaning about 244 Wh/m^2 was used subsequently to reduce the heating load.

For the control strategy based on the zone operative temperature control, the calculated variables were $C_{ADR,D} = 240 \text{ Wh/m}^2$ and $BEFI_D = 61 \text{ W/m}^2$ for the downward case and $C_{ADR,U} = 297 \text{ Wh/m}^2$ and $BEFI_U = 97 \text{ W/m}^2$ for the upward case. The storage efficiency for this case was $\eta_{ADR} = 73\%$ for the rest of the day after the upward flexibility event, meaning about 216 Wh/m^2 was used subsequently to reduce the heating load.

Therefore, it was observed that the control strategy based on air temperature results in a significantly higher energy flexibility compared with the floor surface temperature or operative temperature control. For the downward flexibility, with air temperature control there was a 20% increase compared with the floor surface temperature, and for the upward case an increase of 30% was observed. This is an important consideration in the design of control strategies for the zones with radiant floor system where higher energy flexibility is a major objective.

It was observed that increasing the window to wall ratio (WWR) results in 17% increase in the downward flexibility which is due to the general increase in the reference heating load when the WWR was increased. Moreover, a 42% decrease in upward flexibility was observed.

The effect of solar gains was also investigated, and it was observed that for the case of floor surface temperature control strategy, a 6.5% decrease in downward flexibility and 4% increase in the upward flexibility were observed. The major difference for this case is utilizing the solar gains during the day for a significant increase in the zero load hours which is about 11 h compared with 4 h for the cloudy day.

For future work, it is suggested to perform experimental studies for implementation in large buildings equipped with high-mass radiant systems which can perform both radiant heating and cooling.

Author Contributions: Conceptualization, A.S.-D. and A.K.A.; methodology, A.S.-D., A.K.A. and U.E.; software, A.S.-D.; validation, A.S.-D. and A.K.A.; formal analysis, A.S.-D. and A.K.A.; investigation, A.S.-D. and A.K.A.; data curation, A.S.-D. and A.K.A.; writing—original draft preparation, A.S.-D. writing—review and editing, A.S.-D., A.K.A., U.E. and E.R.-U.; visualization, A.S.-D.; supervision, A.K.A., U.E. and E.R.-U.; project administration, A.K.A.; funding acquisition, A.K.A., U.E. and E.R.-U. All authors have read and agreed to the published version of the manuscript.

Funding: This research received funding from Dubai Electricity and Water Authority (DEWA) R&D Center for the project on Energy Flexible Buildings and NSERC/Hydro-Quebec Industrial Research Chair as well as Canada Excellence Research Chairs Program (CERC-2018-00005). The APC was funded by DEWA R&D Center.

Institutional Review Board Statement: Not applicable.

Informed Consent Statement: Not applicable.

Acknowledgments: The authors would like to thank Sgouris Sgouridis, director of the DEWA R&D Center, for his valuable comments.

Conflicts of Interest: The authors declare no conflict of interest.

Nomenclature

A_i	Area of surface represented by node i (m^2)		
ADR	Active Demand Response	Q_{ref}	Reference heating power profile
BEFI	Building energy flexibility index	Q_{ADR}	Flexible heating power profile
C_i	Thermal capacitance of node i (J/K)	R_{ij}	Thermal resistance between nodes i and j (m^2K/W)
C_{ADR}	available structural energy storage capacity	R_{inf}	Infiltration thermal resistance (m^2W/K)
k	Thermal conductivity of materials ($W/(m.k)$)	R_W	Thermal resistance of walls
K_p	Proportional control constant ($W/^\circ C$)	T_i	Temperature of node i ($^\circ C$)
l_i	Thickness of surface i (m)	T_{sp}	Air setpoint temperature ($^\circ C$)
Q_{aux}	Auxiliary heating source (W)	T_o	Outdoor temperature ($^\circ C$)
Q_i	Source entering node i (W)	T_{floor}	Floor surface temperature ($^\circ C$)
η_{ADR}	Storage efficiency	T_{window}	Window surface temperature ($^\circ C$)
Q_{max}	Maximum heating capacity (system size)	t	Time

References

1. Narayanan, A.; Mets, K.; Strobbe, M.; Develder, C. Feasibility of 100% renewable energy-based electricity production for cities with storage and flexibility. *Renew. Energy* **2019**, *134*, 698–709. [[CrossRef](#)]
2. Aelenei, D.; Lopes, R.A.; Aelenei, L.; Gonçalves, H. Investigating the potential for energy flexibility in an office building with a vertical BIPV and a PV roof system. *Renew. Energy* **2019**, *189*–197. [[CrossRef](#)]

3. Child, M.; Kemfert, C.; Bogdanov, D.; Breyer, C. Flexible electricity generation, grid exchange and storage for the transition to a 100% renewable energy system in Europe. *Renew. Energy* **2019**, *139*, 80–101. [[CrossRef](#)]
4. English, J.; Niet, T.; Lyseng, B.; Keller, V.; Palmer-Wilson, K.; Robertson, B.; Wild, P.; Rowe, A. Flexibility requirements and electricity system planning: Assessing inter-regional coordination with large penetrations of variable renewable supplies. *Renew. Energy* **2020**, *145*, 2770–2782. [[CrossRef](#)]
5. Lund, P.D.; Lindgren, J.; Mikkola, J.; Salpakari, J. Review of energy system flexibility measures to enable high levels of variable renewable electricity. *Renew. Sustain. Energy Rev.* **2015**, *45*, 785–807. [[CrossRef](#)]
6. el Geneidy, R.; Howard, B. Contracted energy flexibility characteristics of communities: Analysis of a control strategy for demand response. *Appl. Energy* **2020**, *263*, 114600. [[CrossRef](#)]
7. Finck, C.; Li, R.; Zeiler, W. Optimal control of demand flexibility under real-time pricing for heating systems in buildings: A real-life demonstration. *Appl. Energy* **2020**, *263*, 114671. [[CrossRef](#)]
8. Zhou, Y.; Zheng, S. Machine-learning based hybrid demand-side controller for high-rise office buildings with high energy flexibilities. *Appl. Energy* **2020**, *262*. [[CrossRef](#)]
9. Jensen, S.Ø.; Marszal-Pomianowska, A.; Lollini, R.; Pasut, W.; Knotzer, A.; Engelmann, P.; Stafford, A.; Reynders, G. IEA EBC Annex 67 Energy Flexible Buildings. *Energy Build.* **2017**, *155*, 25–34. [[CrossRef](#)]
10. Saberi-Derakhtenjani, A.; Athienitis, A.K. Model predictive control strategies to activate the energy flexibility for zones with hydronic radiant systems. *Energies* **2021**, *14*, 1195. [[CrossRef](#)]
11. Hu, M.; Xiao, F.; Jørgensen, J.B.; Li, R. Price-responsive model predictive control of floor heating systems for demand response using building thermal mass. *Appl. Therm. Eng.* **2019**, *153*, 316–329. [[CrossRef](#)]
12. Morovat, N.; Athienitis, A.K.; Candanedo, J.A.; Delcroix, B. Model-Based Control Strategies to Enhance Energy Flexibility in Electrically Heated School Buildings. *Buildings* **2022**, *12*, 581. [[CrossRef](#)]
13. Saberi-Derakhtenjani, A.; Athienitis, A.K. A frequency domain transfer function methodology for thermal characterization and design for energy flexibility of zones with radiant systems. *Renew. Energy* **2021**, *163*, 1033–1045. [[CrossRef](#)]
14. Reynders, G.; Amaral Lopes, R.; Marszal-Pomianowska, A.; Aelenei, D.; Martins, J.; Saelens, D. Energy flexible buildings: An evaluation of definitions and quantification methodologies applied to thermal storage. *Energy Build.* **2018**, *166*, 372–390. [[CrossRef](#)]
15. Brunner, C.; Deac, G.; Braun, S.; Zöphel, C. The future need for flexibility and the impact of fluctuating renewable power generation. *Renew. Energy* **2020**, *149*, 1314–1324. [[CrossRef](#)]
16. Arteconi, A.; Mugnini, A.; Polonara, F. Energy flexible buildings: A methodology for rating the flexibility performance of buildings with electric heating and cooling systems. *Appl. Energy* **2019**, *251*, 113387. [[CrossRef](#)]
17. Hu, M.; Xiao, F. Quantifying uncertainty in the aggregate energy flexibility of high-rise residential building clusters considering stochastic occupancy and occupant behavior. *Energy* **2020**, *194*, 116838. [[CrossRef](#)]
18. Li, H.; Wang, Z.; Hong, T.; Piette, M.A. Energy flexibility of residential buildings: A systematic review of characterization and quantification methods and applications. *Adv. Appl. Energy* **2021**, *3*, 100054. [[CrossRef](#)]
19. le Dréau, J.; Heiselberg, P. Energy flexibility of residential buildings using short term heat storage in the thermal mass. *Energy* **2016**, *111*, 991–1002. [[CrossRef](#)]
20. Foteinaki, K.; Li, R.; Heller, A.; Rode, C. Heating system energy flexibility of low-energy residential buildings. *Energy Build.* **2018**, *180*, 95–108. [[CrossRef](#)]
21. Weiß, T.; Fulterer, A.M.; Knotzer, A. Energy flexibility of domestic thermal loads—A building typology approach of the residential building stock in Austria. *Adv. Build. Energy Res.* **2019**, *13*, 122–137. [[CrossRef](#)]
22. Reynders, G.; Diriken, J.; Saelens, D. Quantifying the active demand response potential: Impact of dynamic boundary conditions. In Proceedings of the 12th REHVA World Congress, Aalborg, Denmark, 22–25 May 2016.
23. Engels, J.; Claessens, B.; Deconinck, G. Optimal Combination of Frequency Control and Peak Shaving With Battery Storage Systems. *IEEE Trans. Smart Grid* **2020**, *11*, 3270–3279. [[CrossRef](#)]
24. Zhou, Y.; Cao, S. Energy flexibility investigation of advanced grid-responsive energy control strategies with the static battery and electric vehicles: A case study of a high-rise office building in Hong Kong. *Energy Convers. Manag.* **2019**, *199*, 111888. [[CrossRef](#)]
25. Foteinaki, K.; Li, R.; Péan, T.; Rode, C.; Salom, J. Evaluation of energy flexibility of low-energy residential buildings connected to district heating. *Energy Build.* **2020**, *213*, 109804. [[CrossRef](#)]
26. Athienitis, A.; Dumont, E.; Morovat, N.; Lavigne, K.; Date, J. Development of a Dynamic Energy Flexibility Index for Buildings and Their Interaction with Smart Grids. 2020 Summer Study on Energy Efficiency in Buildings. 2020. Available online: <https://www.researchgate.net/publication/343725542> (accessed on 1 April 2022).
27. MacDougall, P.; Ran, B.; Huitema, G.B.; Deconinck, G. Performance assessment of black box capacity forecasting for multi-market trade application. *Energies* **2017**, *10*, 1673. [[CrossRef](#)]
28. Candanedo, J.; Dehkordi, V.; Lopez, P. A Control-Oriented Simplified Building Modelling Strategy. In Proceedings of the 13th Conference of International Building Performance Simulation Association, Chambéry, France, 25–28 August 2013.
29. Kim, D.; Braun, J.E. Reduced-order building modeling for application to model-based predictive control 23. In Proceedings of the Simuild 2012, Fifth National Conference of IBPSA-USA, Madison, WI, USA, 1–3 August 2012. Available online: <https://www.researchgate.net/publication/272295068> (accessed on 20 May 2022).

30. Candanedo, J.A.; Vallianos, C.; Delcroix, B.; Date, J.; Derakhtenjani, A.S.; Morovat, N.; John, C.; Athienitis, A.K. Control-oriented archetypes: A pathway for the systematic application of advanced controls in buildings. *J. Build. Perform. Simul.* **2022**, *1–12*. [CrossRef]
31. Joe, J.; Karava, P.; Hou, X.; Hu, J. Model Predictive Control of a Radiant Floor Cooling System in an Model Predictive Control of a Radiant Floor Cooling System in an Office Space. In Proceedings of the International High-Performance Buildings Conference, West Lafayette, IN, USA, 11–14 July 2016. Available online: <http://docs.lib.psu.edu/ihpbc/221> (accessed on 1 March 2022).
32. Candanedo, J.A.; Saberi-Derakhtenjani, A.; D’Avignon, K.; Athienitis, A.K. A pathway for the derivation of control-oriented models for radiant floor heating applications. In Proceedings of the eSim 2018 10th Conference of IBPSA-Canada, Montréal, QC, Canada, 9–10 May 2018.
33. Athienitis, A.K.; O’Brien, W. *Modelling, Design and Optimization of Net-Zero Energy Buildings*; Wiley Ernst & Sohn: Berlin, Germany, 2015.
34. ASHRAE. Measurement of Energy and Demand Saving. In *Guideline 14-2014*; American Society of Heating, Ventilating, and Air Conditioning Engineers: Atlanta, GA, USA, 2014.
35. ASHRAE. Thermal Environmental Conditions for Human Occupancy. In *Standard 55*; American Society of Heating, Ventilating, and Air Conditioning Engineers: Atlanta, GA, USA, 2017.